Eur. Phys. J. B **33**, 47–54 (2003)
DOI: 10.1140/epjb/e2003-00140-5

THE EUROPEAN PHYSICAL JOURNAL B

Polar Kerr rotation of the ferromagnet EuB_6

S. Broderick[1], L. Degiorgi[1,a], H.R. Ott[1], J.L. Sarrao[2], and Z. Fisk[2]

[1] Laboratorium für Festkörperphysik, ETH Zürich, 8093 Zürich, Switzerland
[2] NHMFL-FSU, Tallahassee FL 32306, USA

Received 30 January 2003 / Received in final form 21 March 2003
Published online 23 May 2003 –

Abstract. Magneto-optical data on EuB_6, a ferromagnet with a Curie temperature $T_C \sim 15$ K, are presented and discussed in detail. We have measured the polar Kerr rotation, covering a spectral range from the infrared up to the ultraviolet, as a function of temperature between 1.5 and 20 K and in external magnetic fields between 0 and 10 T. The Kerr rotation in high fields and at low temperatures is enormous. Our observations, which implicitly reflect the large magnetoresistive effects, are shown to discriminate between the spectroscopic response of localized and itinerant electronic states. Our data analysis is based on the phenomenological Lorentz-Drude model, following from the classical dispersion theory and appropriately extended to magneto-optical experiments.

PACS. 78.20.Ls Magnetooptical effects – 75.50.Cc Other ferromagnetic metals and alloys

1 Introduction

Various experimental investigations have recently revealed new and unexpected aspects of ferromagnetism. Particularly intriguing are the hexaborides with divalent M^{2+} cations [1]. For instance, EuB_6 is a ferromagnet with an $S = 7/2$ $4f$-electron local-moment and a Curie temperature T_C of 15.5 K, whereas La-doped CaB_6 is a weak ferromagnet with rather small ordered moments of 0.1 μ_B/La or less, but Curie temperatures in the range between 600 and 1000 K [1,2]. Unexpected experimental results, obtained in various studies of these materials, revitalized the discussion on the possible causes for ferromagnetism in general, a continuing controversial issue in solid state physics [3–7].

Recently, we have focused our attention on EuB_6. According to specific heat data [8,9], the onset of ferromagnetism occurs *via* two-phase transitions and neutron diffraction indicates that the magnetic moments align only sluggishly with decreasing temperature in zero magnetic field [10]. Parallel to a substantial reduction of the zero field electrical resistivity by two orders of magnitude, a significant blue shift of the plasma frequency is observed in the optical reflectivity as the temperature is reduced to below T_C [8]. The unusually drastic response of the conduction electron system to ferromagnetic order is also reflected in large magnetoresistive effects in the range of T_C and below [11]. Furthermore, the magnitude and the temperature dependence of the electrical resistivity suggests that EuB_6 is close to a metal-insulator transition. Thus, EuB_6 is obviously a model system for studying the ferromagnetic state, in particular the corresponding roles of localized moments and conduction electrons and their polarizations. Because of similarities to properties of transition metal oxides [12], the ordered state of EuB_6, due to the spontaneous alignment of the local $4f$ electron moments of the Eu^{2+} ions [10], is also of particular interest. In the paramagnetic state the temperature dependence of the electrical resistivity is of metallic character but the concentration of itinerant charge carriers is low [13]. It is therefore not a priori clear whether the spontaneous alignment of the localized moments is simply due to the usual Ruderman-Kittel-Kasuya-Yoshida (RKKY) interaction or whether other coupling mechanisms might be of significance.

Magneto-optical (MO) experiments and particularly the Kerr effect spectroscopy are suitable for investigating the dependence of the electronic excitation spectrum on the degree of magnetic order. Besides being a bulk sensitive probe of the dynamical response of solids over a broad spectral range, the optical Kerr effect depends on the spin-polarization of the charge carriers and thus provides an elegant method to distinguish spin-polarized states from unpolarized ones.

In this paper we offer a fairly complete set of MO-Kerr data on EuB_6 and its analysis, which provides the rather unique possibility of discriminating between itinerant and localized optical responses and indeed opens new perspectives in studying ferromagnetism in metals. Our discussion is based on previously published results of MO experiments [14]. We complement our previous report with a phenomenological analysis of the data based on the classical (Drude-Lorentz) dispersion theory. This approach allows for extracting some relevant physical parameters, which will be discussed in connection with other experimental observations. First, we briefly address some

[a] e-mail: degiorgi@solid.phys.ethz.ch

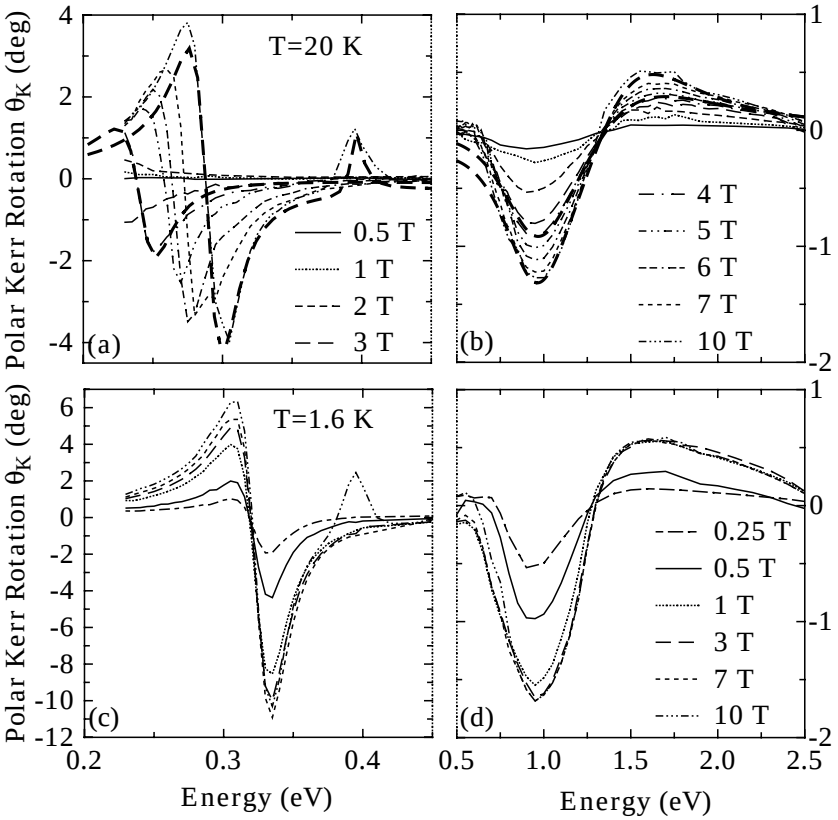

Fig. 1. Experimental polar Kerr rotation spectra of EuB_6 between 0.2 and 2.5 eV at (a–b) 20 and (c–d) 1.6 K as a function of magnetic fields. The thick dashed lines in (a) and (b) are phenomenological fits for 4 and 10 T at 20 K, based on the Lorentz-Drude model (see text). Note that both the energy and the Kerr-rotation scales change from (a) to (b) and from (c) to (d).

experimental details and present a summary of the data. Subsequently, we introduce the Lorentz-Drude approach adapted to analyse MO results. A short summary concludes our paper.

2 Experiment and results

The MO-Kerr measurement is an ellipsometric type of spectroscopy, which measures the characteristics of the axial anisotropy induced by the magnetization of the sample. Here, we consider a polar geometry where the light beam is parallel to the external magnetic field. Linearly polarized light, a superposition of left and right circularly polarized components (LCP and RCP, respectively) of equal magnitude, is reflected from the surface of a single crystal. For EuB_6 this was done at a given temperature between 1.5 and 20 K and in an external field between 0 and 10 T. Because of the non-zero magnetization, the polarization plane of the reflected light is rotated by a field and temperature dependent angle with respect to that of the incident light. This Kerr rotation is due to the differing absorptions for the two circular polarizations and is expressed by the azimuthal polarization rotation θ_K and the polarization ellipticity ϵ_K. Below, we present our measurements of θ_K, defined as:

$$\theta_K = -\frac{1}{2}\left(\Delta_+ - \Delta_-\right) = -\mathrm{Im}\left(\frac{\tilde{n}_+ - \tilde{n}_-}{\tilde{n}_+\tilde{n}_- - 1}\right) \qquad (1)$$

where $\Delta_\pm$ are the phases of the complex reflectance $r_\pm(\omega) = \rho_\pm e^{i\Delta_\pm}$ and $\tilde{n}_\pm = n_\pm - ik_\pm$ are the complex refraction indices for LCP (−) and RCP (+) light, respectively [15]. The formal details pertaining to the Kerr rotation phenomenon have extensively been described elsewhere [15,16].

Figure 1 summarizes the Kerr-rotation data of EuB_6 at 20 and 1.6 K as a function of magnetic field [14]. Two distinct features may be recognized. They are a rather strong and sharp resonance around 0.3 eV and a broader signal at about 1 eV, respectively. The additional feature at 0.4 eV is observed at 10 T only and its amplitude increases with decreasing temperatures. At 20 K we note a remarkable blue shift and an increasing intensity, *i.e.*, a growing Kerr rotation, with increasing magnetic field for the resonance at 0.3 eV. The field dependent blue shift is only moderate at 6 K (not shown here [14]) and essentially absent at 1.6 K. Also at these low temperatures, the intensity of the Kerr rotation at 0.3 eV grows with increasing magnetic field. The maximum rotation of about $-11°$ at 10 T and 1.6 K, is among the very largest Kerr rotations ever observed [16]. The resonance at about 1 eV does not shift in energy but its intensity does change with either decreasing temperature or increasing magnetic field. At 20 K the polar Kerr rotation at 1 eV is enhanced by increasing fields and saturates above 7 T. In the case of

1.6 K and 6 K (not shown here [14]) this saturation occurs already at fields as low as 1 T.

We have also performed reflectivity ($R(\omega) = r(\omega)r^*(\omega) = \rho^2$) measurements at selected temperatures and as a function of magnetic field from the infrared up to the ultraviolet spectral range. Since those findings were presented in detail and extensively discussed elsewhere [17], we just recall them here in view of the discussion below. In close analogy with the temperature dependence [8], we have found a remarkable blue shift of the reflectivity plasma edge with increasing magnetic field at $T > T_C$. This magnetic-field induced blue-shift also saturates at low temperatures.

3 Discussion

3.1 Classical dispersion theory

The standard phenomenological approach to the optical response of solids, based on the classical dispersion theory [18], *i.e.*, the so-called Lorentz-Drude model, can be extended to treat the case where localized and itinerant electrons are being exposed to an externally applied magnetic field H [15,16]. With respect to the situation in zero field, the optical conductivity may be associated with RCP and LCP light and hence is split up into two components σ_+ and σ_-, respectively. For a transition at ω_j, the optical conductivity is

$$\tilde{\sigma}_\pm = \frac{\omega_{pj}^2}{4\pi} \frac{\mathrm{i}\omega}{\omega_j^2 \pm \omega\omega_{cj} - \omega^2 + \mathrm{i}\gamma_j\omega}, \tag{2}$$

with ω_{pj}^2 as the oscillator strength of the excitation, ω_{cj} as the corresponding cyclotron frequency, and γ_j as the related scattering rate. In such a classical model the effects of spin-dependent selection rules and occupation of states are not taken into account. To overcome these shortcomings one can introduce weight-factors $f^\pm$ for the oscillator strengths of RCP and LCP, respectively [16,19]. The complete response is then

$$\tilde{\sigma}_\pm = \sum_j f_j^\pm \frac{\omega_{pj}^2}{4\pi} \frac{\mathrm{i}\omega}{\omega_j^2 \pm \omega\omega_{cj} - \omega^2 + \mathrm{i}\gamma_j\omega}, \tag{3}$$

where the sum is over all optically active excitations j and $f_j^+ + f_j^- = 2$ guarantees the conservation of the total spectral weight [16]. Since $\tilde{\sigma}_\pm = \tilde{\sigma}_{xx} \pm \mathrm{i}\tilde{\sigma}_{xy}$, the diagonal and off-diagonal optical conductivities are

$$\tilde{\sigma}_{xx} = \sum_j \frac{\mathrm{i}\omega\omega_{pj}^2}{8\pi} \frac{(f_j^+ + f_j^-)(\omega_j^2 - \omega^2 + \mathrm{i}\gamma_j\omega) - (f_j^+ - f_j^-)\omega\omega_{cj}}{(\omega_j^2 - \omega^2 + \mathrm{i}\gamma_j\omega)^2 - (\omega\omega_{cj})^2} \tag{4}$$

and

$$\tilde{\sigma}_{xy} = \sum_j \frac{\omega\omega_{pj}^2}{8\pi} \frac{(f_j^+ - f_j^-)(\omega_j^2 - \omega^2 + \mathrm{i}\gamma_j\omega) - (f_j^+ + f_j^-)\omega\omega_{cj}}{(\omega_j^2 - \omega^2 + \mathrm{i}\gamma_j\omega)^2 - (\omega\omega_{cj})^2}. \tag{5}$$

The Drude contribution of the itinerant charge carriers is obtained by setting $\omega_j = 0$ and the corresponding oscillator strength is the squared plasma frequency $\omega_{pD}^2 = 4\pi ne^2/m^*$ (n is the density and m^* is the effective mass of the itinerant particles). There are two major regimes: the first one with $f_j^+ = f_j^- = 1$, known as the "diamagnetic" absorption and the second one with $f_j^+ \neq f_j^-$, known as the "paramagnetic" absorption [15,16]. As will be discussed below, the weight-factors $f^\pm$ are phenomenologically related to the magnetization of the investigated system. It is also easy to verify that for $H = 0$ and $f_j^+ = f_j^- = 1$, equation (4) reduces to the Lorentz-Drude model in zero-field [18]. For a discussion beyond the phenomenological Lorentz-Drude approach, the interested reader may consult reference [20] for an ample and thorough theoretical treatment of the MO Kerr spectra.

Summarizing, since

$$\tilde{n}_\pm^2 = (n_\pm - \mathrm{i}k_\pm)^2 = \epsilon_\infty - \frac{\mathrm{i}4\pi}{\omega}(\tilde{\sigma}_{xx} \pm \mathrm{i}\tilde{\sigma}_{xy}) = \epsilon_\infty - \frac{\mathrm{i}4\pi}{\omega}\tilde{\sigma}_\pm \tag{6}$$

we can use equations (4, 5) for calculating $\tilde{n}_\pm$ by application of equation (6) and correspondingly θ_K from equation (1) (ϵ_∞ is the dielectric optical constant [18]). Consequently, this allows to achieve a phenomenological Lorentz-Drude fit of the measured Kerr rotation θ_K. In particular equation (6) allows for a complete calculation of all optical functions over a broad spectral range [19].

3.2 Fit results

The parameters in equations (4, 5) were determined such that the best possible fits to the experimental curves $\theta_K(\omega)$, shown in Figure 1, were obtained. One Drude component for the response due to the itinerant charge carriers and three harmonic oscillators (h.o.) were used. Two h.o.'s at ∼0.9 and ∼1.2 eV are necessary in order to reproduce the experimental features of $\theta_K(\omega)$ between 0.8 and 2.5 eV. The third h.o. at 6 eV was introduced in order to account for the spectral weight above our upper experimentally accessible frequency limit of 5 eV, and it is kept constant at all fields and temperatures. The same applies for the dielectric optical constant ϵ_∞, which accounts for the high-energy electron interbands contribution to the optical properties. The parameters of the h.o. at 6 eV and ϵ_∞ were determined in order to allow a better reproducibility, both qualitatively and quantitatively, of the temperature and magnetic field independent reflectivity spectra above 1 eV (see Ref. [8] for $R(\omega)$ up to 12 eV and Ref. [21] for $R(\omega)$ up to 30 eV). While the h.o. at 6 eV and ϵ_∞ have a purely phenomenological meaning, the purpose of these latter two fit components is obviously to account for the so-called screening due to the high energy interband transitions [18], affecting both $R(\omega)$ and $\theta_K(\omega)$ in the spectral range reached by our measurements [22]. An additional fourth h.o. at 0.4 eV has been considered for the feature observed only at 10 T (see Fig. 1). In our preliminary analysis [14], a simpler version of the model was considered consisting of only one h.o. around 1 eV.

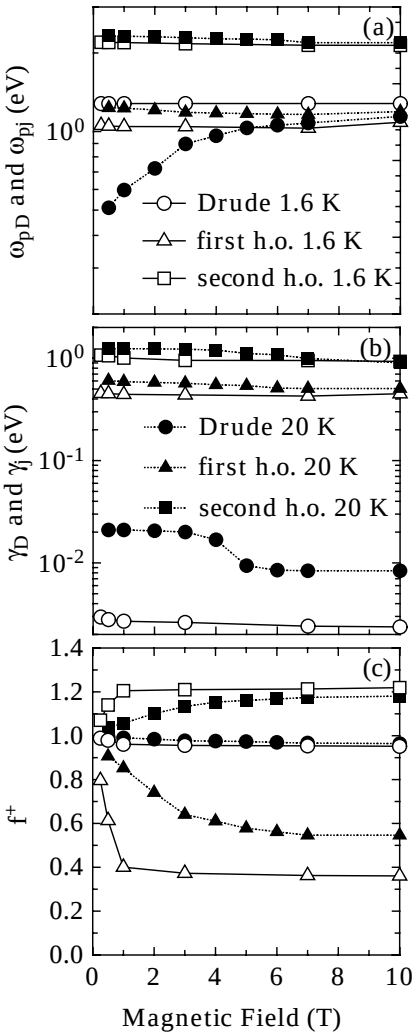

Fig. 2. Magnetic field dependence of selected fit parameters at 1.6 and 20 K (see also Tab. 1 and Ref. [23]): (a) Drude plasma frequency (ω_{pD}) and oscillator strengths (ω_{pj}), (b) Drude (γ_D) and h.o. scattering rates (γ_j) and (c) weight-factors (f_j^+) of the Drude and h.o. components at ∼0.9 (first) and 1.2 eV (second). The corresponding symbols for the various components are the same in all panels. Note the logarithmic y-axis scales in panel (a) and (b). The lines are guide to the eyes.

While the main features and trends were reproduced (see *e.g.* inset of Fig. 1 in Ref. [14]) the fit quality in $\theta_K(\omega)$ was not so satisfactory and the reproduction of the reflectivity spectra was rather poor, as well.

Despite the large amount of fit-parameters, it turns out that the set of parameters, that provides the best reproduction of the experimental data, is rather unique and different fit-procedures converged to the same final results. We established distinct trends in the field dependences of the relevant fit-parameters such as the Drude and oscillator strengths, the $f^{\pm}$-factors and the scattering rates. Figure 2 graphically summarizes the magnetic field dependence of these fit-parameters at 20 and 1.6 K, which turn out to be the most significant quantities determining the temperature and magnetic field dependence of the magneto-optical properties. In Table 1 all fit parameters are listed for magnetic fields of 1 and 10 T, and of 4 and 10 T at 1.6 and 20 K, respectively [23]. The magnetic field and temperature dependences of the fit parameters are discussed in more detail in the next sections. Here, we notice that the h.o. resonance frequencies barely change as a function of temperature and field, and that $\omega_{cj} = eH/m^*c$ is set by the experimental magnetic field H and was kept constant for all h.o.'s. Even though the effective mass m^* of the charge carriers may vary with magnetic field [17], we set $m^* = m_e$. This is justified because the energy scale set by ω_{cj} is so small with respect to the spectral range discussed here that the values of ω_{cj} and their dependence on m^* are not critical for the fit procedure and results.

Figures 3a–b and 4a–b show the calculated magnetic field dependences of $\sigma_{1xy}(\omega)$ and $\sigma_{2xy}(\omega)$ at 20 K, respectively. The Drude component as well as the feature around 1 eV grow progressively with increasing magnetic field. Figures 3c–d and 4c–d illustrate the contributions of the Drude component and of the three h.o.'s to the total off-diagonal conductivity at 1.6 K and 10 T. Figures 5a and b

Table 1. Lorentz-Drude fit parameters for equations (3–5) at 1.6 and 20 K, and at selected magnetic fields of 1 and 10, and 4 and 10 T, respectively: ϵ_∞ for the optical dielectric constant, ω_c for the cyclotron frequency, ω_{pD} and γ_D for the Drude plasma frequency and scattering rate, and ω_j, ω_{pj}, and γ_j for the resonance frequency, oscillator strength and scattering rate of the Lorentz h.o.'s, and, finally, the f_j^+ for the weight factor of the RCP light.

fit	1.6 K		20 K	
parameters	1 T	10 T	4 T	10 T
ϵ_∞	8.15	8.15	8.15	8.15
ω_{pD} (eV)	1.28	1.28	0.964	1.14
γ_D (eV)	0.00269	0.00237	0.0169	0.00838
f_D^+	0.961	0.952	0.975	0.964
ω_1 (eV)	0.893	0.908	0.889	0.896
ω_{p1} (eV)	1.045	1.09	1.18	1.19
γ_1 (eV)	0.444	0.45	0.551	0.506
f_1^+	0.401	0.361	0.611	0.546
ω_2 (eV)	1.20	1.21	1.23	1.26
ω_{p2} (eV)	2.19	2.14	2.27	2.19
γ_2 (eV)	1.01	0.931	1.20	0.902
f_2^+	1.21	1.22	1.15	1.18
ω_3 (eV)	6	6	6	6
ω_{p3} (eV)	10	10	10	10
γ_3 (eV)	6	6	6	6
f_3^+	1	1	1	1
ω_4 (eV)	-	0.395	-	0.394
ω_{p4} (eV)	-	0.048	-	0.045
γ_4 (eV)	-	0.007	-	0.01
f_4^+	-	2	-	2
ω_c (eV)	1.16×10^{-4}	0.00116	4.63×10^{-4}	0.00116

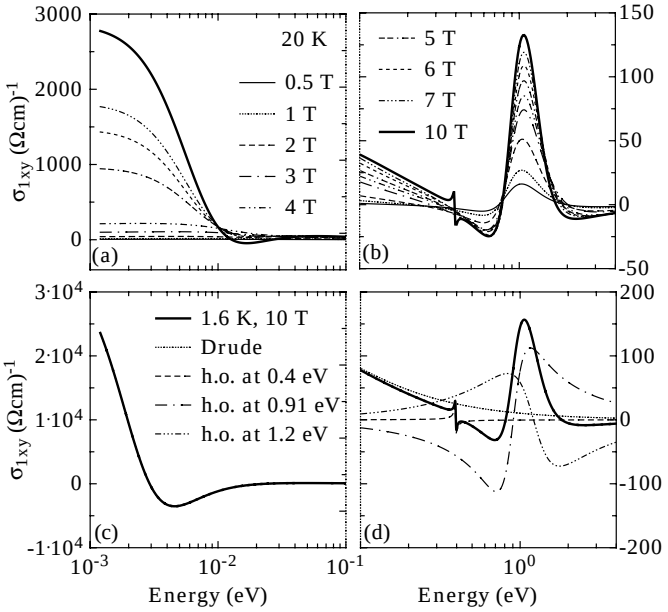

Fig. 3. (a–b) Real part of the off-diagonal component of the conductivity tensor at 20 K as a function of magnetic field, calculated from the Lorentz-Drude model. Panels (c) and (d) highlight individual fit components of the same quantity at 1.6 K but at 10 T only. In panel (c) only the Drude component is shown. It fully determines σ_{1xy}, since the contribution of the h.o.'s is basically zero in this spectral range. Note that both the energy and the y-axis scales change from (a) to (b) and from (c) to (d).

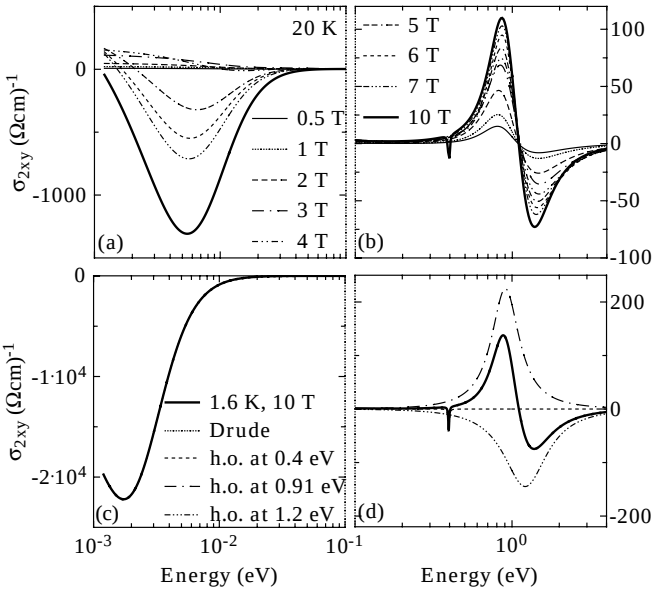

Fig. 4. (a–b) Imaginary part of the off-diagonal component of the conductivity tensor at 20 K as a function of magnetic field, calculated from the Lorentz-Drude model. Panels (c) and (d) highlight individual fit components of the same quantity at 1.6 K but at 10 T only. In panel (c) only the Drude component is shown. It fully determines σ_{2xy}, since the contribution of the h.o.'s is basically zero in this spectral range. Moreover, panel (d) displays the contribution of the three h.o.'s only, since the Drude component is here vanishingly small. Note that both the energy and the y-axis scales change from (a) to (b) and from (c) to (d).

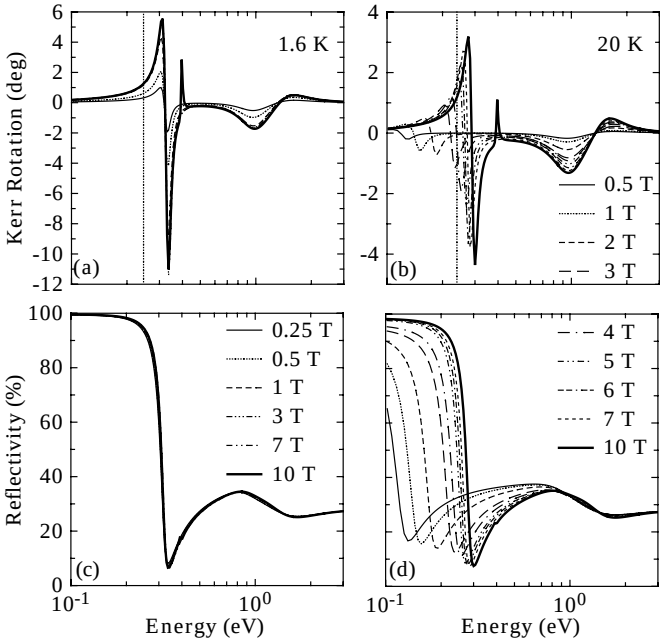

Fig. 5. (a–b) Calculated polar Kerr rotation and (c–d) calculated optical reflectivity at 1.6 and 20 K at various magnetic fields from 0.1 up to 3 eV. The low energy limit of the Kerr spectrometer (*i.e.*, 0.23 eV) is marked with a vertical thin dotted line. Note that the Kerr-rotation scales are not the same in (a) and (b). Note that no shift of $R(\omega)$ is obtained and observed at 1.6 K [17].

display the calculated θ_K at 1.6 and 20 K as a function of magnetic field and covering the spectral range between 0.1 and 3 eV. The calculated extension below the measurable photon energy interval is meant to illustrate the expected evolution of θ_K below the experimental limit of 0.23 eV, particularly for $T = 20$ K. The calculations employing the chosen fit parameters reproduce the experimental results of θ_K almost perfectly. Since this remarkable agreement cannot be appreciated very well in Figure 5, we also compare the experimental curves with the corresponding calculated Kerr rotations (thick dashed lines) at 4 and 10 T at 20 K in Figure 1. The same quality of agreement is achieved for all combinations of temperature and magnetic field.

Another rigorous test of our fits to the θ_K spectra is to check the consistency between the reflectivity spectra calculated from the θ_K fit-parameters and the measured reflectivity data. Figures 5c and d show the calculated magnetic field variation of the reflectivity spectra at 1.6 and 20 K, obtained with the parameters of Table 1 and those of reference [23]. The calculated $R(\omega)$ spectra are in fair agreement with the measured data, which were obtained independently and discussed elsewhere [8,17]. Especially well reproduced is the blue shift of the plasma edge in $R(\omega)$ at 20 K and its saturation at 1.6 K with increasing magnetic field [14,17]. The behaviour from the plasma edge up to 1 eV of $R(\omega)$ both in temperature and magnetic field is also qualitatively very well recovered by this simple phenomenological model. Around 1 eV, the calculated $R(\omega)$ is about 5 to 10% larger than the

measured one. Since the goal was here to demonstrate the intimate relationship between θ_K and $R(\omega)$, we did not attempt a fine adjustment of the fit variables in order to force a better agreement between measured and calculated $R(\omega)$. Nevertheless, it is worth noting that even the trend of the calculated $R(\omega)$ above 5 eV agrees with the measured data [8,21]. The agreement with the experimental $R(\omega)$ data also gives us confidence that the calculated trend in θ_K below the present experimental limit of 0.23 eV is likely to be observed in experiments.

3.3 Magneto-optics of EuB_6

The successful phenomenological Lorentz-Drude fits to θ_K and $R(\omega)$ indicate an important interplay between the components that influence the measured Kerr rotation. The interplay between the localized-electron interband transitions (here around 1 eV), represented by Lorentz harmonic oscillators, and the free-electron response in the form of a Drude term, leads to a strong resonance in the polar Kerr rotation (in this case at energies of about 0.3 eV) coinciding with the reflectivity plasma edge [16,24]. The relevance of this situation was first suggested by Feil and Haas [25], but not entirely recognized or correctly interpreted in previous work [15,26,27]. The claim of Feil and Haas [25] was based on model calculations, also employing the classical dispersion theory. The dispersion of the diagonal part of the dielectric constant near the plasma edge in a metallic material has a strong influence on the MO properties. The plasma edge itself leads to resonance-like peaks in the Kerr rotation and to a strong enhancement of the magnitude of the Kerr effect. The calculations by Feil and Haas were based on the assumption that $\tilde{\sigma}_{xy}$ is energy-independent thus adopting a constant value. This is obviously incompatible with the Kramers-Kronig relation [25,26]. We note that our phenomenological calculations are general in the sense that they are *not* limited by the assumption of Feil and Haas and satisfy the self-consistency requirements of the Kramers-Kronig relations [16]. Our data on EuB_6 as well as the phenomenological discussion based on the extended Lorentz-Drude model represent the most detailed and comprehensive experimental confirmation to date of the interplay among the Drude resonance and the interband transition in shaping the Kerr spectra, as originally postulated by the concept of Feil and Haas. The generality of our phenomenological approach goes beyond the debate and controversy [26], raised by the original theory [25].

Therefore, both the Drude component and the two h.o.'s around 1 eV are essential for reproducing the overall features of the experimental θ_K. The shape of the resonance in θ_K at energies coinciding with the onset of the reflectivity plasma edge (*i.e.*, $\sim$0.3 eV) as well as the sign of θ_K around 1 eV are the direct consequence of the appropriate choice of the corresponding $f^{\pm}$-factors. The h.o.'s around 1 eV are strongly polarized, *i.e.*, $f_j^{\pm} \neq 1$, while the polarization of the Drude component deviates only little from the diamagnetic limit $f^{+} = 1$ (Fig. 2c). The absolute intensity of the Kerr rotation features is then given by the corresponding distribution of spectral weights, *i.e.*, the Drude plasma frequency and the oscillator strengths, shown in Figure 2.

3.3.1 Interband transitions

The feature in θ_K at about 1 eV is ascribed to electronic interband transitions, involving the localized f-electron states of the Eu^{2+} ions. The optical conductivity exhibits a variety of features between 1 and 10 eV [8,21]. In particular, the absorption at 1 eV was previously [21] interpreted as an exciton-type transition between localized $4f$ and more extended $5d(e_g)$ states. While we cannot explain, why two phenomenological h.o.'s around 1 eV are necessary, it could well be that the complexity of the band structure involving degenerate f and d states leads to transitions with excitation energies close to 1 eV.

Band structure calculations [28] as well as direct experimental evidence [9,10] confirm that the localized magnetic moment is due to the seven electrons in the localized $4f$-shell of the Eu^{2+} ions. Above T_C, *i.e.*, at 20 K, the moments of the localized $4f$ states are aligned by the magnetic field while below T_C the spontaneous ferromagnetic state orders these moments. This scenario accounts for the progressive growth of the 1 eV resonance at 20 K and the saturation of its intensity as a function of magnetic field at 1.6 K. At 20 K, a high magnetic field is required for inducing a (Zeeman) splitting of the localized states, larger than the thermal energy scale set by the temperature. Consequently, the Kerr rotation grows only gradually. Below T_C, relatively low fields are sufficient to align the magnetic moments almost completely and thus the Kerr rotation does not grow significantly with increasing fields. Still puzzling is the feature at 0.4 eV, which suddenly develops at a field of 10 T. We suggest that it might represent the Kerr response induced by the spin-orbit splitting of the states involved in the $4f-5d(e_g)$ transition at 1 eV.

From the phenomenological fit we infer that the scattering rates (γ_j) of the two h.o.'s at 0.9 and 1.2 eV are magnetic-field independent but slightly decrease with decreasing temperature (Fig. 2b). The oscillator strength of the h.o. at 1.2 eV is also temperature and magnetic field independent, while the one for the oscillator at about 0.9 eV remains almost constant in field but decreases with decreasing temperature (Fig. 2a). This latter behaviour partially accounts for the shift of spectral weight into the Drude component (see below).

Our previous arguments supporting the assignment of the Kerr rotation feature at 1 eV to excitations involving localized electronic states were based on a comparison of the field dependence of the Kerr rotation (*i.e.*, peak to peak amplitudes) at different temperatures with the field induced bulk magnetization (see Fig. 4 of Ref. [14]). It turns out that the Kerr amplitudes at 1 eV, normalized by the respective values measured at 1.6 K and 10 T, which were assumed to be the saturation values, exhibit the same general trend as the $M(H)$ curves at all temperatures. This observation is consistent with our interpretation of associating the 1 eV signal with transitions between

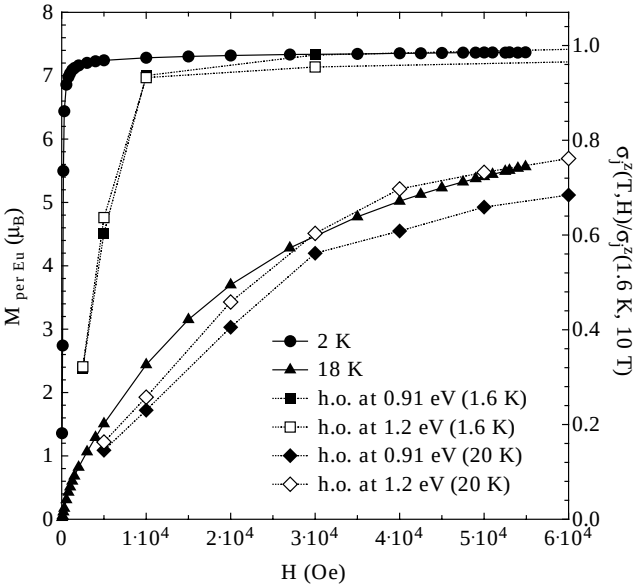

Fig. 6. Comparison between the measured magnetization [29] and the ratio $\sigma_j^z(T,H)/\sigma_j^z(1.6\text{ K}, 10\text{ T})$, appropriately scaled to $M(H)$ at selected temperatures (see text).

localized $4f$ and more extended $5d$ electron states. These are certainly directly influenced by the bulk magnetization, which is dominated by the polarization of the local $4f$-electron moments [10].

By exploiting our phenomenological fits, this conclusion may now be put on even firmer ground. As already mentioned, the $f^{\pm}$-factors in equations (3–5) can be related to the magnetization. In our phenomenological approach, $f_j^{\pm}\omega_{pj}^2$ defines the relative weight associated with the charges involved in the optical transitions for RCP and LCP light, respectively. Consequently, a simple two level scenario of Zeeman splitting leads to a situation where f^+ and f^- represent the distribution of spectral weight among up and down spin states, respectively. Therefore, we define the quantity $\sigma_j^z \sim |(f^+ - f^-)/(f^+ + f^-)| = |f^+ - 1|$ (with the condition that $f_j^+ + f_j^- = 2$, see above), representing the effective spectral weight redistribution between the RCP and LCP transitions. It is instructive to compare $M(H)$ with the ratio $\sigma_j^z(T,H)/\sigma_j^z(1.6\text{ K}, 10\text{ T})$ of the two h.o.'s at 0.9 and 1.2 eV. This is shown in Figure 6, where those ratios have been scaled to the saturation level of $M(H)$ at low T and high H, *i.e.*, unity on the right-hand y-axis of Figure 6 coincides with the saturation magnetization of EuB_6. The comparison of the two quantities in Figure 6 at high and low temperatures is very good and both quantities follow the same evolution both in temperature and field. This confirms the claimed relation between the magnetic moments of the localized $4f$ states and their Kerr response.

3.3.2 Intraband transitions

We now focus our attention on the Kerr rotation signal around 0.3 eV, mainly due to the response of the itinerant electrons. In Figure 5 we compare the calculated Kerr response with the calculated reflectivity as a function of field for two selected temperatures. The $R(\omega)$ spectra calculated on the basis of the Lorentz-Drude model agree very nicely, both qualitatively and quantitatively, with the experimental results [8,17]. The temperature and the magnetic field induced shifts of the reflectivity plasma edge are strikingly similar. With either decreasing temperature in zero field or with increasing field at constant temperature, the plasma edge exhibits an unusual and remarkable blue shift [30]. The field-induced blue shift is considerable at $T > T_C$ but is progressively reduced below T_C. This is clearly reflected in the magnetic field dependence of the Drude plasma frequency ω_{pD} at 20 and 1.6 K in Figure 2a. The (unscreened) plasma frequency ω_{pD} tends to a constant value at low temperatures and high magnetic fields. The temperature and field dependences of ω_{pD}, evaluated from our fits to θ_K (Fig. 2a), are in good agreement with our previous values, directly extracted from the measured $R(\omega)$ spectra (Fig. 2 in Ref. [17]). The Drude scattering rate γ_D (Fig. 2b) is strongly reduced between 20 and 1.6 K at all fields. Nevertheless, apart from a weak reduction of γ_D around 4 T at 20 K, the magnetic field dependence of γ_D at fixed temperature is rather weak. This might indicate that spin-flip processes are not significant [7,17].

Considering the present data set it seems natural to conclude that the 0.3 eV Kerr rotation is tied to the reflectivity plasma edge around 0.3 eV. The blue shifts of both the plasma edge and the Kerr rotation signal are a direct spectroscopic manifestation of the dynamical response of the free charge carriers in the ferromagnetic state and therefore correlate with features of the (large) magnetoresistance [11,17]. The obvious "pinning" of the θ_K resonance at 0.3 eV to the blue shift of the $R(\omega)$ plasma edge provides a convincing experimental confirmation of the above mentioned theoretical conjecture of Feil and Haas [25,26].

As in the discussion for the 1 eV feature in θ_K, we can similarly compare the MO-Kerr response at 0.3 eV to $M(H)$. It was shown (Fig. 4 of Ref. [14]) that the field-induced growth of the renormalized Kerr amplitude at 0.3 eV is much more gradual than that of the 1 eV signal. Such a gradual increase of the Kerr amplitude at 0.3 eV with respect to the magnetization curves, particularly at higher temperatures, was supposed to reflect the only indirect influence of the internal field due to local moments on the spin polarization of the conduction electrons. The negligible redistribution of spectral weight between RCP and LCP light for the Drude components (*i.e.*, the $f^{\pm}$-factors for the Drude term barely deviate from 1, as shown in Fig. 2c) implies that the itinerant charge carriers are not relevant in shaping the bulk $M(H)$ curves.

4 Conclusion

The MO-Kerr response of EuB_6 exhibits distinct features at different energies, which are both strongly dependent on temperature and external magnetic fields. The polar Kerr rotation of EuB_6 turns out to be among the very

largest ever observed and exhibits the same blueshift as the reflectivity. This is tantamount to a temperature and field dependent change of "color" of this material. Moreover, the MO results are a spectroscopic manifestation of the very large magnetoresistive effects of EuB_6.

Using an extension of the Lorentz-Drude phenomenology, we have separated the contributions of itinerant and localized charges. This provides a spectroscopic access to the magnetic state of the system, and allows to identify the direct consequences of ferromagnetism on relevant quantities, such as the optical spectral weight (plasma frequency and oscillator strengths). We found that only the localized charge carriers show any substantial polarization. This is also demonstrated by the correlation between the MO-response of the itinerant and localized states and the bulk magnetization. Therefore, EuB_6 is a model system in order to study the interplay between itinerant and localized states, putting on firmer ground the general interpretation of Kerr spectra, after the argument of Feil and Haas [25].

The authors wish to thank F. Salghetti-Drioli and F. Lucchinetti for collecting data during a preliminary stage of the project, and J. Hirsch, R. Monnier, L. Cooper, D. Basov and S. Signoretti for fruitful discussions. This work has been supported by the Swiss National Foundation for the Scientific Research.

References

1. H.R. Ott, J.L. Gavilano, B. Ambrosini, P. Vonlanthen, E. Felder, L. Degiorgi, D.P. Young, Z. Fisk, R. Zysler, Physica B **281-282**, 423 (2000), and references therein
2. D.P. Young, D. Hall, M.E. Torelli, Z. Fisk, J.L. Sarrao, J.D. Thompson, H.R. Ott, S.B. Oseroff, R.G. Goodrich, R. Zysler, Nature **397**, 412 (1999).
3. C. Herring, in *Magnetism*, edited by G.T. Rao, H. Suhl, Vol. IV (Academic Press, New York, 1966)
4. T. Moriya, J. Magn. Magn. Mat. **14**, 1 (1979)
5. A.J. Millis, P.B. Littlewood, B.I. Shraiman, Phys. Rev. Lett. **74**, 5144 (1995)
6. J.C. Cooley, M.C. Aronson, J.L. Sarrao, Z. Fisk, Phys. Rev. B **56**, 14541 (1997)
7. J.E. Hirsch, Phys. Rev. B **62**, 14131 (2000) and references therein
8. L. Degiorgi, E. Felder, H.R. Ott, J.L. Sarrao, Z. Fisk, Phys. Rev. Lett. **79**, 5134 (1997)
9. S. Süllow, I. Prasad, M.C. Aronson, J.L. Sarrao, Z. Fisk, D. Hristova, A.H. Lacerda, M.F. Hundley, A. Vigliante, D. Gibbs, Phys. Rev. B **57**, 5860 (1998)
10. W. Henggeler, H.R. Ott, D.P. Young, Z. Fisk, Solid State Commun. **108**, 929 (1998)
11. C.N. Guy, S.v. Molnar, J. Etourneau, Z. Fisk, Solid State Commun. **33**, 1055 (1980)
12. S. Jin, T.H. Tiefel, M. McCormack, R.A. Fastnacht, R. Ramesh, L.H. Chen, Science **264**, 413 (1994)
13. S. Paschen, D. Pushin, M. Schlatter, P. Vonlanthen, H.R. Ott, D.P. Young, Z. Fisk, Phys. Rev. B **61**, 4174 (2000)
14. S. Broderick, L. Degiorgi, H.R. Ott, J.L. Sarrao, Z. Fisk, Eur. Phys. J. B **27**, 3 (2002)
15. W. Reim, J. Schoenes, in *Ferromagnetic Materials*, edited by K.H.J. Buschow, E.J. Wohlfarth, Vol. 5 (Elsevier Science, 1990), p. 133
16. F. Salghetti-Drioli, Ph.D. thesis Nr. 13393 (1999), ETH-Zurich (`http://e-collection.ethbib.ethz.ch/cgi-bin/show.pl?type=diss&nr=13393&lang=`) and references therein
17. S. Broderick, B. Ruzicka, L. Degiorgi, H.R. Ott, J.L. Sarrao, Z. Fisk, Phys. Rev. B **65**, 121102(R) (2002)
18. F. Wooten, in *Optical Properties of Solids* (Academic Press, New York, 1972), M. Dressel, G. Grüner, in *Electrodynamics of Solids* (Cambridge University Press, 2002)
19. S. Broderick, Ph.D. Thesis Nr. 14969, ETH Zurich (unpublished)
20. P.M. Oppeneer, in *Handbook of Magnetic Materials*, edited by K.H.J. Buschow, Vol. 13 (Elsevier Science, 2001), p. 229
21. S. Kimura, T. Nanba, M. Tomikawa, S. Kunii, T. Kasuya, Phys. Rev. B **46**, 12196 (1992)
22. ϵ_∞ is rather large since it accounts for several interband transitions occuring in the spectral range above 10 eV. Alternatively, we could have set $\epsilon_\infty = 1$ and introduced more h.o.'s besides the one at 6 eV. In order to reduce the amount of fit parameters, we have adopted a more phenomenological fit procedure
23. Complete tables with the full set of parameters at 1.6, 6 and 20 K for all measured magnetic fields are available at the link: (`http://www. solidphys.ethz.ch/spectro/suppinfo/EuB6-KerrFit.pdf`)
24. F. Salghetti-Drioli, P. Wachter, L. Degiorgi, Solid State Commun **109**, 773 (1999)
25. H. Feil, C. Haas, Phys. Rev. Lett. **58**, 65 (1987)
26. J. Schoenes, W. Reim, Phys. Rev. Lett. **60**, 1988 (1988) and H. Feil, C. Haas, Phys. Rev. Lett. **60**, 1989 (1988)
27. R. Pittini, J. Schoenes, O. Vogt, P. Wachter, Phys. Rev. Lett. **77**, 944 (1996)
28. S. Massidda, A. Continenza, T.M. de Pascale, R. Monnier, Z. Phys. B **102**, 83 (1997)
29. We use here the magnetization data obtained with a standard magnetometer by Paschen *et al.* (unpublished) on the same sample. These results are in perfect agreement with similar data by S. Süllow *et al.* (Ref. [9])
30. To our knowledge, EuB_6 is the first example for such a blue shift of the plasma edge as a function of both temperature and magnetic field. A much weaker blue shift of the plasma edge has also been seen as a function of temperature *only*, in ferromagnetic semimetals, like TbN: P. Wachter, F. Bommeli, L. Degiorgi, P. Burlet, F. Bourdarot, E. Kaldis, Solid State Commun. **105**, 675 (1998)